

http://pubs.acs.org/journal/aelccp

In Situ Growth of a Metal—Organic Framework-Based Solid Electrolyte Interphase for Highly Reversible Zn Anodes

Ziqi Wang,* Huige Chen, Huashan Wang, Weiyuan Huang, Hongyan Li,* and Feng Pan*



Cite This: ACS Energy Lett. 2022, 7, 4168–4176



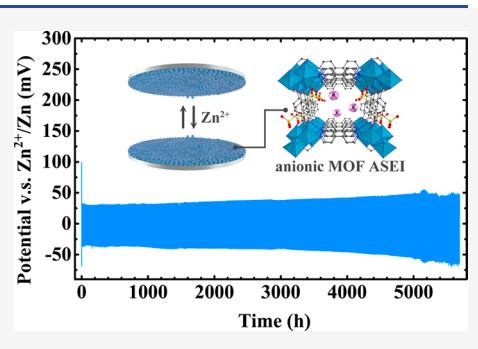
ACCESS I

Metrics & More

Article Recommendations

s) Supporting Information

ABSTRACT: Aqueous Zn ion batteries are receiving tremendous attention owing to their attractive features with respect to safety, cost, and scalability, yet their lifespan is severely limited by the poor reversibility of the Zn metal anode. Thereby, an artificial solid electrolyte interphase (ASEI) based on an anionic metal—organic framework (MOF) is in situ fabricated on the surface of Zn anodes. The robust ASEI protects the anode from side reactions and largely promotes its Coulombic efficiency during battery cycling. Owing to the high intrinsic Zn^{2+} conductivity and abundant zincophilic sites, it also facilitates enhanced Zn redox activities. More interestingly, the consecutive sulfonate groups in the MOF channels guide rapid and directional transport of Zn ions and thus endow a dendrite-free Zn plating/stripping lifespan of 5700 h at 2 mA cm $^{-2}$.



This work provides a fresh strategy to promote the performance of Zn and even other metallic anodes toward practical battery applications.

ovel battery chemistries are constantly being explored to meet the high requirements in terms of energy density, safety, and cost for the next generation of energy storage systems. Recently, aqueous zinc ion batteries (AZIBs) have gained increasing attention owing to their merits, such as high capacity, good safety, eco-friendliness, and low cost, which are ideal for large-scale energy storage and wearable devices.^{1,2} Metallic Zn is the best choice for the anode material of AZIBs considering its high theoretical capacity (820 mAh g^{-1}), suitable potential (-0.76 V versus standard hydrogen electrode), and relative stability in aqueous electrolytes.^{3,4} Nevertheless, the poor reversibility of Zn anodes severely restricts the practicability of AZIBs. To be specific, Zn dendrites are usually generated during cycling due to random ion diffusion and sluggish ion replenishment. This not only brings the risk of battery short-circuit but also causes "dead" Zn and rapid capacity fading.5 Meanwhile, the parasitic hydrogen evolution reaction (HER) at the surface of Zn anodes brings down the Coulombic efficiency (CE) and induces battery swelling upon prolonged cycling. Moreover, the HER also leads to an increase in localized pH because of the consumption of protons, which triggers the formation of electrochemically inert compounds, such as Zn hydroxides and oxides.^{6,7} These byproducts in turn reduce the active area for Zn plating/stripping and thus slow down the redox kinetics and induce inhomogeneous growth of Zn. Hence, the in-depth investigation of improving the reversibility of Zn anode is essential for the development of AZIBs.

The above notorious problems of Zn anodes stem from the absence of a solid electrolyte interphase (SEI) in aqueous electrolytes. In nonaqueous energy storage systems such as Li-, Na-, and K-ion batteries, the decomposition of organic electrolytes in situ produces a film-like SEI covering the anode. ^{8,9} It prevents interface deterioration by hindering further reactions between the anode and the electrolyte, provided that the SEI is physically/chemically stable throughout battery operation. ^{10,11} In AZIBs, however, the decomposition of aqueous electrolytes only results in gas release and inactive byproducts. Therefore, constructing an artificial SEI (ASEI) on the surface is a feasible approach to enhancing the stability of Zn metal anodes. ¹² A successfully designed ASEI can not only increase the kinetic overpotential for HER but also guide uniform Zn²⁺ flux. ^{13,14} Moreover, a robust ASEI is highly desirable to restrain the dendrite growth of Zn. ¹⁵

One routine strategy to introduce an ASEI is directly coating functional (in)organic materials on the surface of Zn. For instance, dendrite-free Zn metal anodes were obtained with a nano-CaCO₃ coating owing to its porous nature to regulate

Received: August 30, 2022 Accepted: October 20, 2022 Published: October 27, 2022





ACS Energy Letters http://pubs.acs.org/journal/aelccp Letter

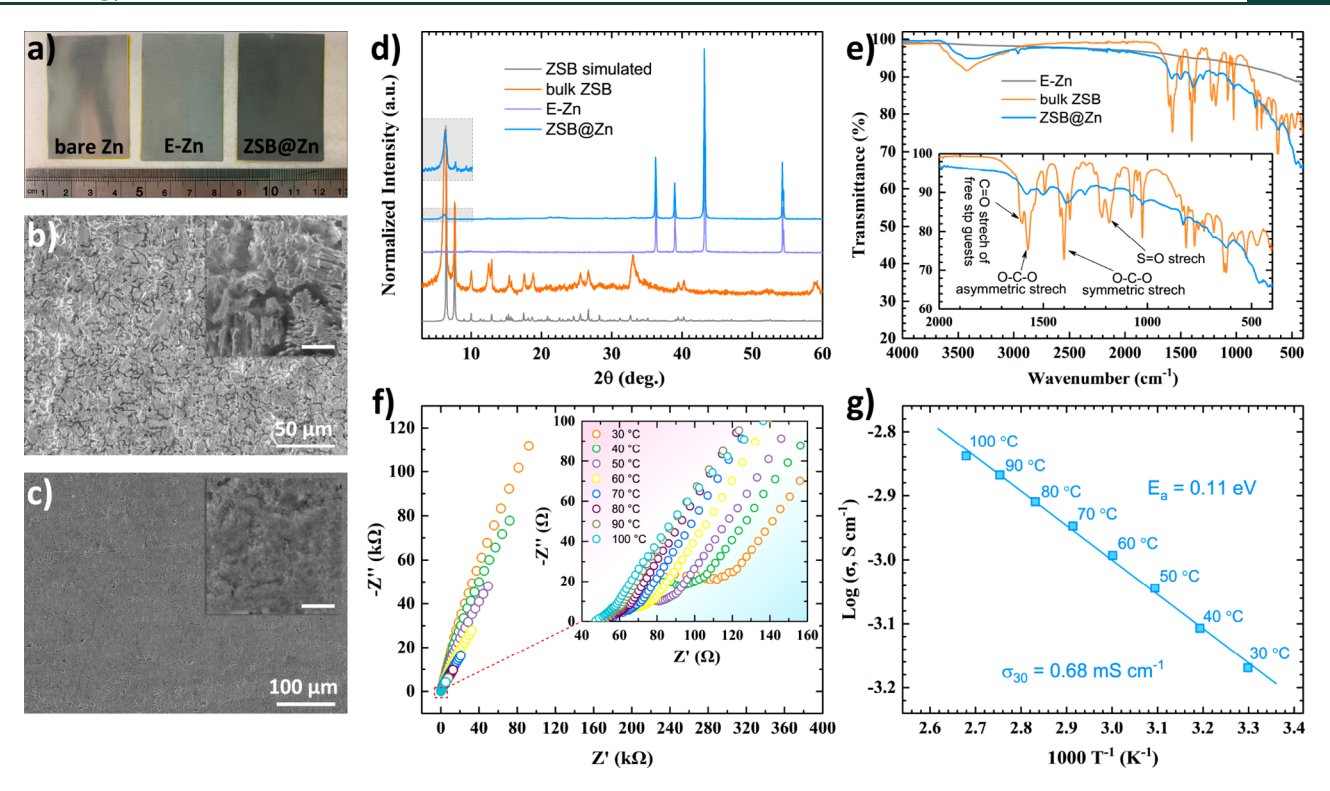


Figure 1. (a) Digital photographs of bare Zn, E-Zn, and ZSB@Zn. SEM images of the (b) E-Zn and (c) ZSB@Zn. Scale bar of the insets: 10 µm. (d) XRD patterns of the simulated ZSB, bulk ZSB, E-Zn, and ZSB@Zn. (e) FTIR of the synthesized ZSB, E-Zn, and ZSB@Zn. (f) EIS profiles of ZSB at temperatures from 30 to 100 °C and (g) corresponding Arrhenius plot of the ionic conductivity.

homogeneous Zn plating/stripping. 16 For the similar purpose, protective coatings based on ZrO2, 17 BaTiO2, 18 TiN, 19 polyamide, 20 gelatin, 21 and so on have been extensively investigated in recent years. The target ASEI can be readily fabricated on Zn anodes through the coating method, but it lacks a strong chemical interaction with the Zn anode to retain a steady interfacial contact during repeated plating/stripping. Another commonly used strategy to integrate an ASEI on Zn anodes is adding SEI-forming additives in aqueous electrolytes. 22,23 The SEI layer is in situ derived from the additives, which firmly adhere to the surface of Zn through chemical bindings. The challenge lies in the deliberate design of a suitable SEI-forming chemistry to meet the following criteria of an ideal ASEI. First, the ASEI must remain intact during cycling in order to provide sustained protection for the Zn anode. Second, high ionic conductivity is preferred to promote the Zn redox kinetics. Third, to avoid dendrite growth, it should demonstrate a high modulus and regulate uniform Zn²⁺ flux.

With such considerations in mind, here we propose room-temperature (RT) self-assembly of a metal—organic framework (MOF) based ASEI on Zn anodes. The MOF layer tightly adheres to the surface of Zn through coordination bonds, ensuring good interfacial integrity during battery operation. It demonstrates a high intrinsic Zn²⁺ conductivity of 0.68 mS cm⁻¹ at 30 °C, which significantly promotes the electrochemical activity of Zn anodes. More important, benefiting from its abundant one-dimensional (1D) anionic channels, the MOF ASEI regulates uniform Zn deposition, and thus results in steady plating/stripping performance for 5700 h. Such merits of the MOF ASEI are analyzed in detail through a series of electrochemical tests and density functional theory (DFT) calculations. When coupled with a vanadium oxide cathode, the

full Zn-ion battery simultaneously delivers enhanced cycling stability over 2000 cycles and rate capability up to 10 A g⁻¹.

The conceptual design and room-temperature synthesis of the MOF ASEI on Zn anodes are schematically depicted in Figure S1. The selected MOF, denoted as ZSB (Zn-stp-bpy), is composed of Zn(II) metal centers with monosodium 2sulfoterephthalate (stp) and 4,4'-bipyridine (bpy) linkers.²⁴ It demonstrates anionic 1D channels with dangling sulfonate groups (Figure S1) that facilitates rapid Zn²⁺ transport. Before the growth of ZSB ASEI, bare Zn anodes were etched with an ammonium persulfate solution to increase reactivity. 25 As shown in Figure 1a, the surface of the etched Zn (E-Zn) tarnishes, and corrosion cracks are observed in the scanning electron microscopy (SEM) morphologies (Figure 1b and S2a), indicating more reactive sites for MOF growth. The integration of the ZSB ASEI was performed through immersing a piece of E-Zn in the precursor solution of MOF. As shown in Figure 1a, the ASEI protected Zn (named as ZSB@Zn) foil remains smooth. When investigated with SEM, densely packed MOF nanoparticles are clearly observed to form a continuous and uniform surface (Figure 1c). Since the E-Zn provides the Zn(II) source for direct MOF growth, the ASEI layer is tightly attached to the Zn substrate through coordination bonds, which is further evidenced by their seamless interfacial contact (Figure S2b,c). As demonstrated in Figure S3 and Supporting Information Video 1, the MOF ASEI can remain intact even under vigorous bending and scratching, indicating superior reliability during battery operation. The mechanical properties of the ZSB ASEI were determined by a microhardness test (Table S1). A high elastic modulus of 11.7 GPa is observed that further confirms its structural robustness. Note that the integration of the ZSB ASEI on Zn anodes is a simple wet chemistry process under ambient

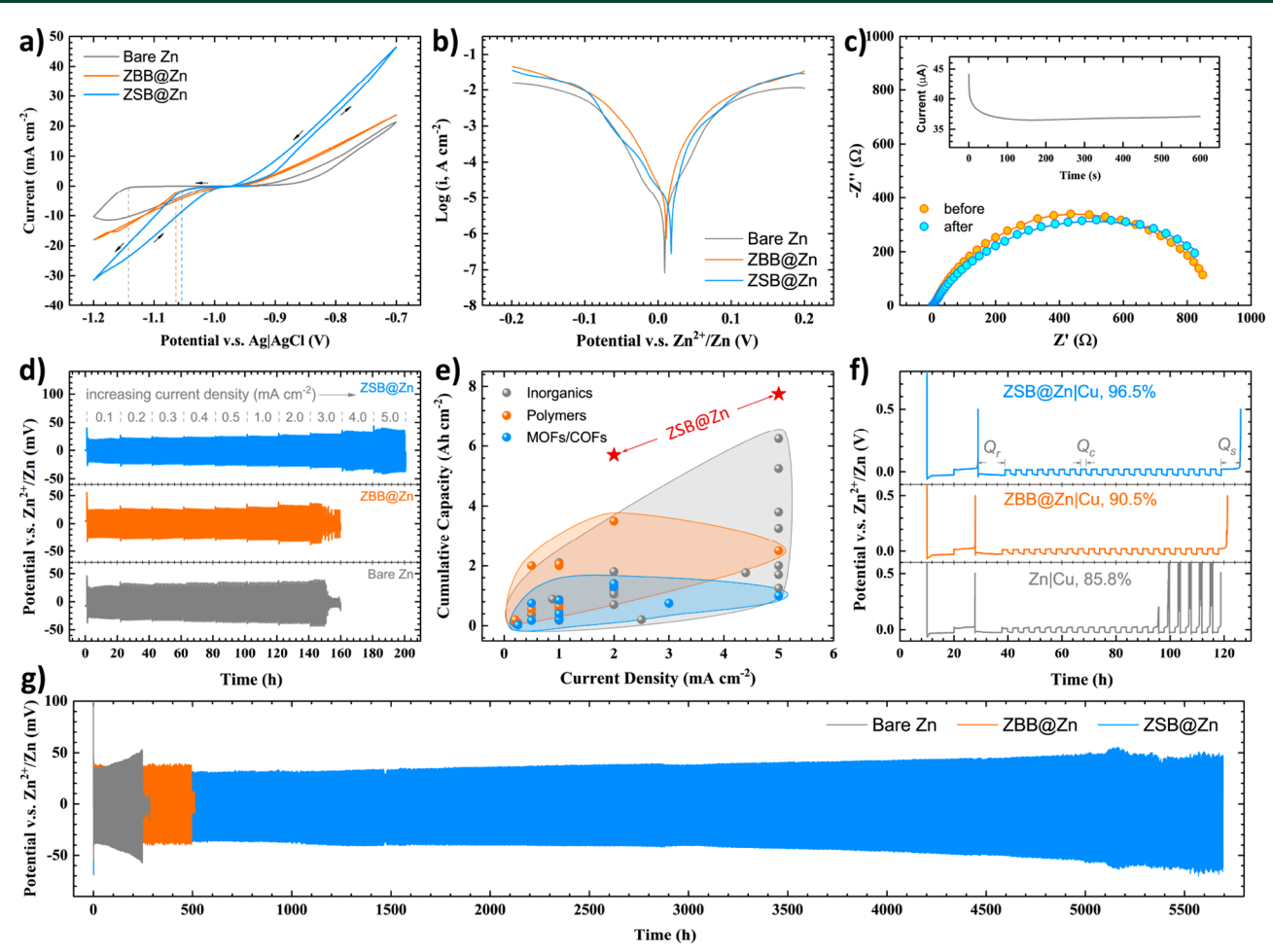


Figure 2. (a) CV curves and (b) Tafel plots of the bare Zn, ZBB@Zn, and ZSB@Zn anodes at a scan rate of 0.5 mV s^{-1} . (c) EIS profiles of the ZSB@Zn symmetric cell before and after polarization under 50 mV. Inset: the corresponding chronoamperometry curve. (d) Zn plating/stripping performance at difference current densities of the symmetric cells. (e) Comparation for the electrochemical performance of the recently reported Zn anodes with functional interphases. (f) Average Coulombic efficiency of the asymmetric cells with bare Zn, ZBB@Zn, and ZSB@Zn anodes. The applied current is 0.5 mA cm^{-2} . (g) Zn plating/stripping performance at 2 mA cm $^{-2}$ of the symmetric cells.

conditions and thus is feasible for roll-to-roll large-scale manufacturing.

The successful growth of ZSB ASEI was conclusively confirmed by the X-ray diffraction (XRD) and Fouriertransform infrared spectroscopy (FTIR) tests. As depicted in Figure 1d and Figure S4, the diffraction peaks of the ZSB@Zn anode at 6.3° and 7.7° are assigned to the ZSB MOF (020) and (200) diffractions, respectively, since they are consistent with the simulated XRD pattern (CCDC No. 663301). Moreover, FTIR absorption peaks of carboxyl and sulfonate groups in the stp ligand can also be distinguished in ZSB@Zn, ^{26,27} as marked in Figure 1e. These results elucidate that the ZSB AESI has an identical crystal structure and chemical properties to the bulk ZSB. The sulfonate groups arranged in the 1D channels of ZSB not only regulate uniform Zn²⁺ flux but also create a Zn²⁺-rich environment for an accelerated anode reaction. Thereby, the Zn²⁺ conductivity of ZSB is further tested by electrochemical impedance spectroscopy (EIS). The counterions in ZSB were replaced by Zn²⁺ in advance via ionic exchange to obtain pure Zn²⁺ conduction.^{28,29} Figure 1f shows the EIS profiles of the bulk ZSB at different temperatures. It demonstrates a high intrinsic Zn²⁺ conductivity of 0.68 mS cm⁻¹ at 30 °C. Accordingly, a small activation energy of 0.11 eV is calculated by following the Arrhenius relationship between conductivity

and temperature (Figure 1g).³⁰ Such high conductivity and small activation energy are highly desirable for good battery performance.

To investigate the positive effect of the dangling sulfonate groups on the electrochemical performance of Zn anodes, an analogue MOF of ZSB, ZBB (Zn-bdc-bpy), was studied as the reference (Figure S5). The framework of ZBB is neutral and does not contain additional Zn²⁺ as counterions. The ZBB@Zn anode was prepared following a procedure similar to that for ZSB@Zn, except that terephthalic acid (bdc) was used as the ligand instead of stp. Its XRD and FTIR profiles are shown in Figure S6. Contact angles of the aqueous electrolyte (1 M zinc triflate) with the ZSB@Zn, ZBB@Zn, and bare Zn anodes are first compared. As shown in Figure S7, the values are 43°, 73°, and 100° for the three anodes, respectively. Apparently, the wettability of the Zn anode has been improved by the MOF ASEI, and the ZSB@Zn shows the smallest contact angle owing to the hydrophilic sulfonate groups. A small contact angle indicates good electrolyte-anode contact for charge transfer, and thus, better redox activity can be envisaged for the ZSB@Zn sample.¹⁴ Symmetric cells were assembled and tested to study the electrochemical performance of the anodes. Figure 2a shows the cyclic voltammetry (CV) curves of the symmetric cells. During the cathodic scan, the Zn²⁺ reduction overpotential of

ACS Energy Letters http://pubs.acs.org/journal/aelccp Letter

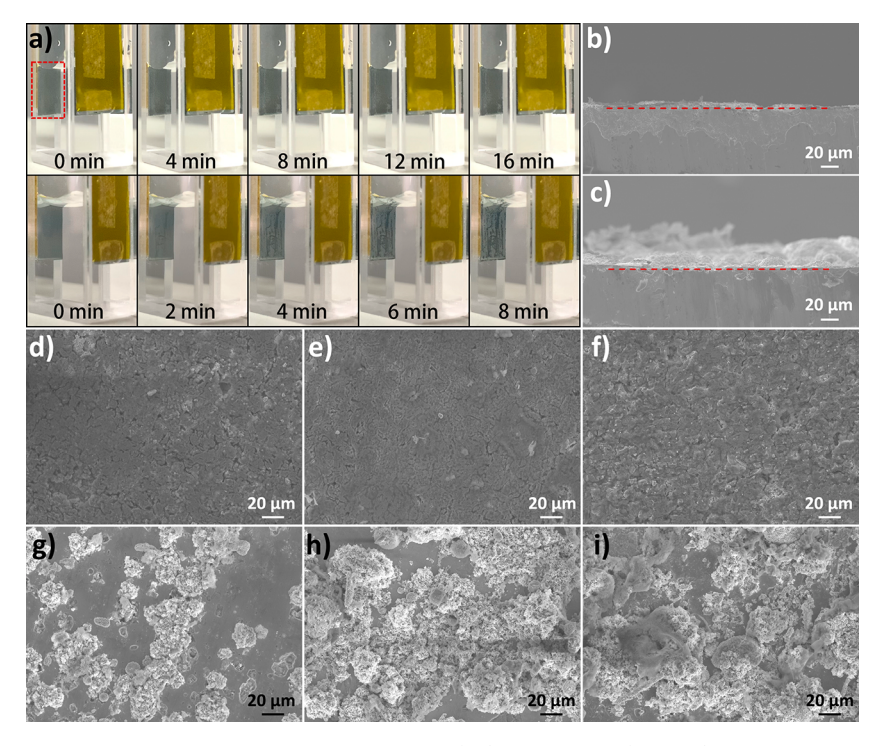


Figure 3. (a) Optical photographs of the Zn deposition on the ZSB@Zn (up) and bare Zn (bottom) anodes at 10 mA cm $^{-2}$. SEM cross-section view of the (b) ZSB@Zn and (c) bare Zn anodes after Zn deposition at 10 mA cm $^{-2}$ for 10 min. SEM images of the ZSB@Zn anode after Zn deposition at 10 mA cm $^{-2}$ for (d) 5, (e) 10, and (f) 15 min, respectively. SEM images of the bare Zn anode after Zn deposition at 10 mA cm $^{-2}$ for (g) 5, (h) 10, and (i) 15 min, respectively.

ZSB@Zn is the lowest, indicating an effectively reduced energy barrier for Zn deposition. Additionally, the more intense peak current observed in the ZSB@Zn cell manifests that the ZSB ASEI facilitates higher electrochemical activity. As shown by the Tafel plots of the anodes (Figure 2b), the corrosion potential of ZSB@Zn positively shifts by 9 mV, but no significant change is seen in the ZBB@Zn sample, indicating the ZSB ASEI can upgrade the resistance against corrosion and the concomitant HER process. Through modulating the ionic flux, the ASEI should have an influence on the transference number of Zn²⁺ $(t_{Z_n})^{2+}$. Here, the Bruce-Vincent method was executed to evaluate $t_{\rm Zn}^{2+}$ for different samples. ³² As shown in Figure 2c and Figure S8, $t_{Zn^{2+}}$ is calculated to be 0.47, 0.58, and 0.63 for the symmetric cells with bare Zn, ZBB@Zn, and ZSB@Zn anodes, respectively (Table S2). Both ZBB and ZSB ASEIs facilitate a higher $t_{Z_n^{2+}}$ by virtue of the well aligned microchannels that regulate the transport of anions and cations.³³ The highest $t_{7n^{2+}}$ is obtained by ZSB@Zn because of the following two reasons. First, the Zn²⁺ counterions in ZSB ASEI increase the number of free cations. Second, the anionic channels act as free pathways for Zn2+ but reject anion transport due to electrostatic interactions.³⁴ The high Zn²⁺ conductivity and transference number synergistically accelerate Zn²⁺ diffusion at the anode/ electrolyte interphase and result in a significantly reduced charge transfer resistance (Figure 2c).

To evaluate the reversibility of the ASEI modified anodes, Zn plating/stripping tests were carried out with the symmetric cells. Figure 2d displays the voltage profiles under different current densities. As the current increases, the bare Zn and ZBB@Zn cells fail at 3.0 mA cm⁻², while the ZSB@Zn cell can survive a high current density of 5.0 mA cm⁻². The results imply that the critical current of the cell is promoted by the ZSB ASEI with fast Zn²⁺ diffusion kinetics. Moreover, under the same current, the

ZSB@Zn cell exhibits a lower overpotential compared with its counterparts. The detailed plating/stripping voltage curves at 2 mA cm⁻² are compared in Figure S9. Figure 2g displays the longterm plating/stripping cycling of the symmetric cells under 2 mA cm⁻². A short circuit triggered by dendrite growth is observed in the bare Zn and ZBB@Zn cells after 250 and 500 h of tests, respectively. While in stark contrast, the ZSB@Zn cell undergoes a stable cycling over 5700 h, suggesting successful dendrite suppression with the ZSB ASEI that regulates uniform Zn²⁺ flux. Besides, the plating/stripping overpotential of the ZSB@Zn roughly remains constant within 3000 h. However, without the protection of the MOF ASEI, the bare Zn anode suffers severe interfacial deterioration as the overpotential increases rapidly upon cycling. Furthermore, a long lifespan of 3100 h is also achieved by the ZSB@Zn anode under a harsh testing condition of 5 mA cm⁻², 2.5 mAh cm⁻² (Figure S10), proving the high reliability of the ZSB ASEI during battery operation. Statistical analysis was performed on the recently reported Zn anodes with functional ASEIs or coatings so as to highlight the unrivalled performance of the ZSB@Zn anode. We classify the protecting layers into three categories: inorganics, polymers, and crystalline porous materials including MOFs and covalent organic frameworks (COFs). Figure 2e summarizes the cumulative capacity of the documented anodes, and our ZSB@ Zn ranks at the top of the list. The details of the recorded references are listed in Table S3. ZnlCu cells were further assembled and tested to study the influence of the MOF ASEI on the Coulombic efficiency of the Zn anode. The average CE of the cell for the first 20 cycles is determined following the method proposed by Xu et al., 35 which is 85.8%, 90.5%, and 96.5% for ZnlCu, ZBB@ZnlCu, and ZSB@ZnlCu, respectively (Figure 2f). Through regulating uniform Zn²⁺ deposition and inhibiting HER, the CE has been effectively promoted by the ZSB ASEI.

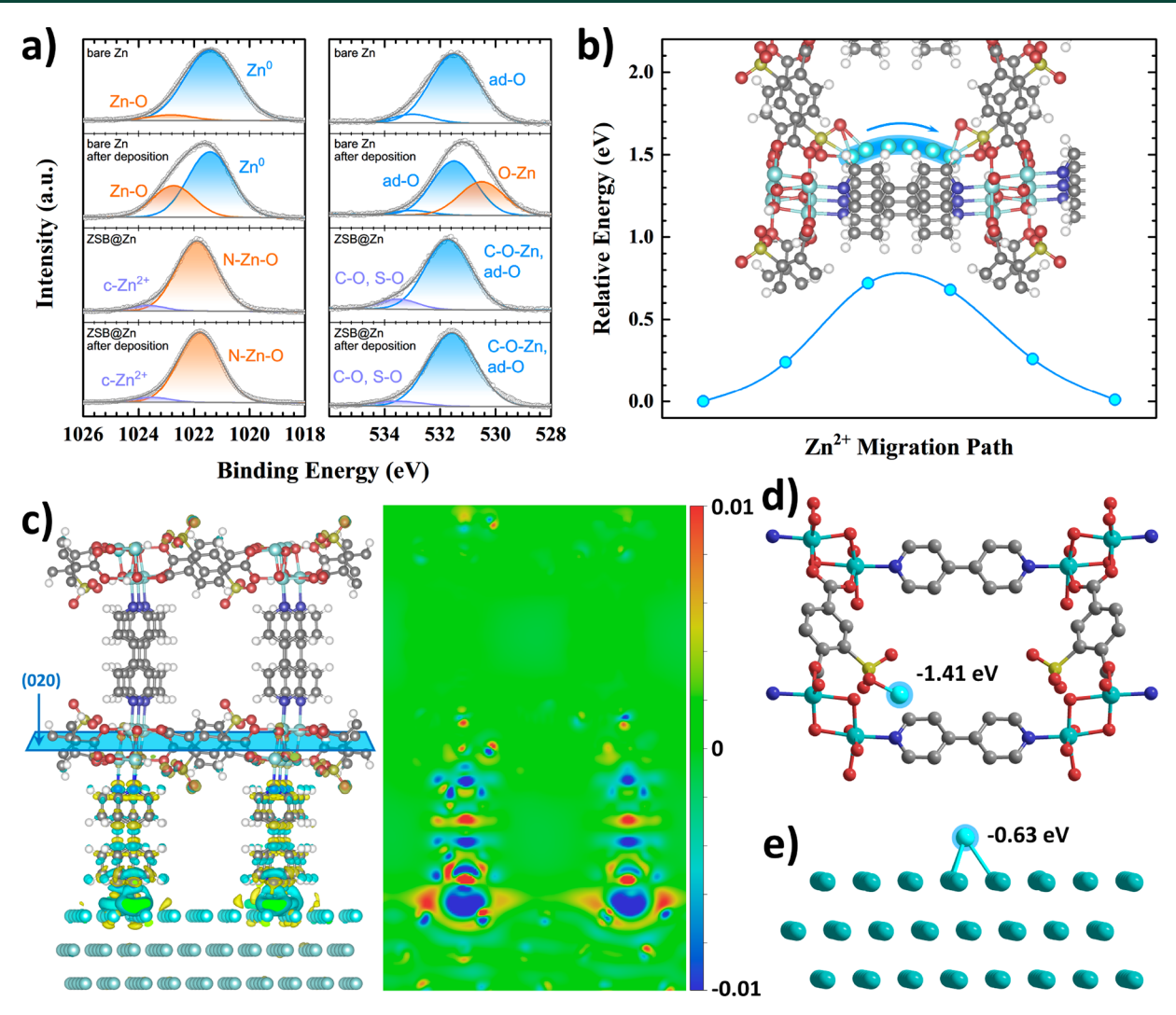


Figure 4. (a) Zn $2p_{3/2}$ (left) and O 1s (right) XPS peaks of the bare Zn and ZSB@Zn anodes before and after plating/stripping test. c-Zn²⁺ represents the Zn²⁺ counterions in the ZSB; ad-O represents the adsorbed oxygen. (b) Energy profile of the calculated Zn²⁺ migration path along the ZSB anionic channels. (c) Charge density difference distribution of the ZSB@Zn interphase (left) and the corresponding sliced 2D contour map (right). The binding energy of a foreign Zn²⁺ at the absorption sites of (d) ZSB ASEI and (e) Zn (002) surface. C, N, O, S, and Zn atoms are represented by gray, blue, red, yellow, and cyan spheres.

Note that without a protective layer, the ZnlCu could hardly accomplish the test due to its low CE. The long-term cycling of the ZSB@ZnlCu cell further indicates that its CE can reach 99.3% after 30 cycles and approach 100% in the following (Figures S11 and S12).

The ability of the ZSB ASEI to guide uniform Zn deposition is further confirmed by the morphology study. We recorded the topography change of the anodes during galvanostatic Zn deposition, as shown in Figure 3a and Supporting Information Video 2 and Video 3. Apparently, the ZSB@Zn remains a smooth surface during the test, indicating that the ZSB ASEI facilitates a homogeneous Zn deposition. However, in the scenario of bare Zn, the unevenly deposited Zn can be clearly distinguished from the substrate and eventually forms a bumpy surface. What is worse, the weakly bonded Zn particles tend to easily flake off and produce "dead" Zn. The morphologies of the deposited Zn were investigated with SEM (Figure 3b,c) are the cross-section views of the ZSB@Zn and the bare Zn anodes after deposition. By virtue of the ZSB ASEI, the deposited Zn on ZSB@Zn is much denser and more homogeneous than on bare Zn. Moreover, the MOF layer was intact during Zn deposition,

as confirmed by the compact and smooth surface in Figure 3d–f. The deposited Zn on the bare Zn, however, suffers from rampant growth (Figure 3g–i). These results stringently corroborate the capability of the ZSB ASEI to guide uniform Zn deposition.

X-ray photoelectron spectroscopy (XPS) was used to study the chemical states of the anodes after repeated Zn plating/ stripping, as shown in Figure 4a. The XPS peaks were assigned according to the previous reports. 36-38 For the bare Zn anode, the peaks corresponding to Zn-O interactions rise in both Zn 2p_{3/2} and O 1s spectra. Combined with the XRD results (Figure S13), the byproduct is determined to be zinc hydroxide triflate. 39,40 It is known that the pH elevation in the AZIBs usually induces the precipitation of zinc hydroxide species.⁴¹ Here, the pH elevation in the symmetric cell suggests an active HER on the bare Zn anode. In contrast, the XPS spectra of ZSB@Zn before and after the test are consistent, meaning that the HER is effectively suppressed. Additionally, we find the deposited Zn is underneath the ZSB ASEI because only the Zn and O signals belonging to ZSB are detected. The integrity of the ZSB ASEI after cycling can also be inferred from its unchanged chemical states. As shown in Figure S13, the XRD of the tested

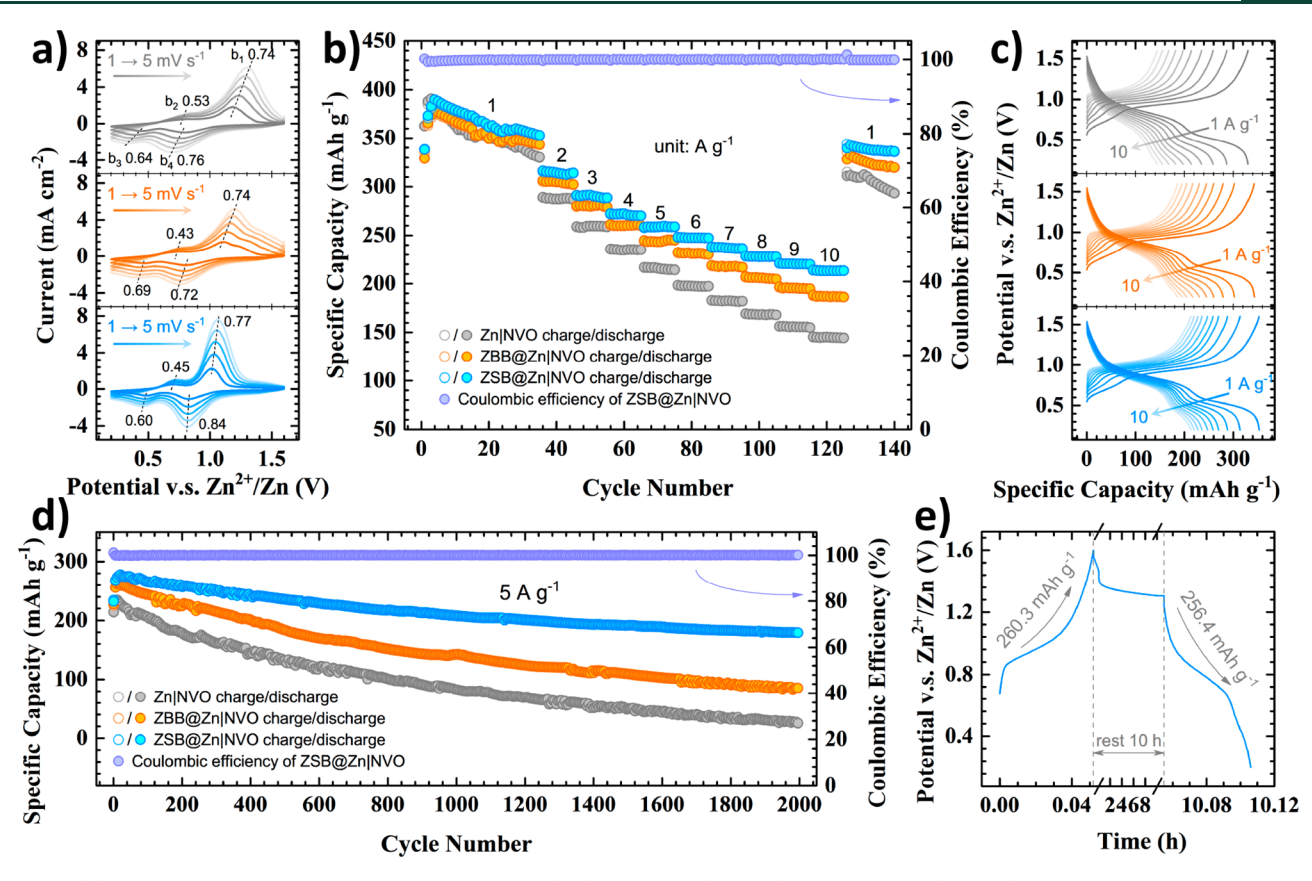


Figure 5. (a) CV profiles of the NVO full cells with bare Zn (top), ZBB@Zn (middle), and ZSB@Zn (bottom) anodes, respectively, at different scan rates. (b) Rate capability and (c) corresponding charge/discharge curves of the NVO full cells with bare Zn, ZBB@Zn, and ZSB@Zn anodes, respectively, at different current densities. (d) Cycling performance of the full cells at 5 A g^{-1} . (e) Self-discharge of the ZSB@ZnlNVO cell at 5 A g^{-1} after 10 h of rest.

ZSB@Zn retains the characteristic diffraction peaks of ZSB, which further proves the high stability of the ZSB ASEI during cycling. Density functional theory (DFT) calculations were subsequently employed to explore the working mechanism of the ZSB ASEI. Figure 4c is the geometrically optimized model of the ZSB@Zn interphase with corresponding charge density difference distribution. The unbalanced charge distribution at the interphase not only accelerates the Zn2+ diffusion but also enhances the adhesion of the ZSB layer to the Zn substrate. 42 The calculation provides a possible way for the connection between ZSB MOF and Zn, namely, through N-Zn coordination bonds. Note that the predicted MOF orientation with its (020) plane parallel to the interface is consistent with the XRD results (Figure 1d and Figure S4), in which (020) is the dominated reflection plane of ZSB. To better elucidate the high intrinsic Zn²⁺ conductivity of the ZSB ASEI, the Zn²⁺ migration paths were simulated. As shown in Figure 4b, we find the migration path between two adjacent sulfonate groups reveals a small energy barrier of about 0.78 eV, indicating that the consecutive sulfonate groups in the MOF channels facilitate rapid and directional transport of Zn ions. Consequently, the high ionic conductivity and uniform Zn²⁺ flux are achieved by the ZSB ASEI. The binding energy of Zn²⁺ on the sulfonate active site is calculated to be -1.41 eV (Figure 4d), much higher than that on bare Zn (-0.63 eV, Figure 4e). The high binding energy of ZSB ASEI suggests a strong zincophilicity at the anode/electrolyte interphase, which contributes enhanced redox kinetics to the anode.⁴³

To assess the reliability of the MOF ASEI for practical applications, full batteries were assembled in coupling with a Na₂V₆O₁₆ (NVO) cathode due to its abundance and high capacity. The phase characterization of the as-prepared Na₂V₆O₁₆ is provided in Figure S14. As expected, saliently improved electrochemical performance has been achieved by the ZSB@ZnlNVO cell owing to the high redox kinetics and reversibility of the ZSB@Zn anode. Figure 5a displays the CV profiles at different scan rates of the ZnlNVO, ZBB@ZnlNVO, and ZSB@ZnlNVO cells, respectively. By virtue of higher interfacial charge transfer at the anode, the ZSB@ZnlNVO cell demonstrates better electrochemical kinetics as indicated by its smaller voltage polarization and more intensive peak currents. No significant improvement is revealed by the ZBB@ZnlNVO cell compared with the control, suggesting the dangling sulfonate groups in the MOF channels are critical to the battery performance. Besides, according to the power law, 44-46 the peak current (i) is correlated to the scan rate (v): $i = av^b$. Once b approaches 0.5, the capacity is mainly attributed to the diffusioncontrolled process, while b close to 1 indicates that a capacitive process is dominated in the capacity contribution. By means of a logarithmic transformation (Figure S15), the b values were calculated and noted in Figure 5a. The main anodic and cathodic peaks of the ZSB@ZnlNVO cell reveal elevated b values, implying an excellent high-rate capability with more capacitive contribution attributed to the anionic ASEI that can store additional Zn2+ ions. The CV curves for the first 5 cycles of the three cells were also compared. As depicted in Figure S16, the ZSB@Zn|NVO cell demonstrates substantially overlapped CV

Letter

curves ascribed to the good reversibility of the anode, while a changing peak current is observed in the ZnlNVO cell due to the instability of bare Zn.

Figure 5b shows the galvanostatic charge/discharge cycling of the three cells at different current densities from 1 to 10 A g^{-1} . They deliver a comparable capacity of about 380 mAh g⁻¹ in the initial cycles (1 A g⁻¹). However, as the current rate increases, the advantages of the ZSB ASEI begin to emerge. At 10 A g^{-1} , the discharge capacity of ZSB@Zn|NVO is 213 mAh g⁻¹, far superior to the cells with ZBB@Zn (186 mAh g^{-1}) and bare Zn (144 mAh g⁻¹) anodes. When the current rate goes back to 1 A g⁻¹, the capacity of all the cells can recover to their initial level. The charge/discharge curves at corresponding current rates are displayed in Figure 5c, and a smaller voltage hysteresis is demonstrated by the ZSB@ZnlNVO cell. Collectively, the rate capability of the full cell is promoted by the ZSB ASEI with enhanced redox activity. The long-term cycling stability of the cells was tested at 5 A g⁻¹. As shown in Figure 5d, after 2000 cycles, the remaining capacities of the cells with ZSB@Zn, ZBB@Zn, and bare Zn anodes are 179, 85, and 25 mAh g⁻¹, respectively. Benefiting from the highly reversible ZSB@Zn anode, the full cell delivers a low capacity fading rate of 0.11 % per cycle. The ZSB ASEI maintained good integrity after cycling (Figure S17), indicating its high stability and ability to suppress dendritic growth. The self-discharge phenomenon commonly exists in AZIBs, which not only decreases CE but also results in the irreversible consumption of electrolyte. 13 The effect of the ZSB ASEI on self-discharge was evaluated by measuring the discharge capacity of a fully charged cell after resting for 10 h. As shown in Figure 5e and Figure S18, the ZSB@ZnlNVO cell releases 98.5% of the original capacity, but the cell with bare Zn exhibits only 81.3%, implying the ASEI layer effectively alleviates the self-discharge behavior. As the full cells were tested parallelly, the above superior electrochemical performance of ZSB@Znl NVO should be attributed to the merits of ZSB ASEI, such as high Zn redox kinetics, good stability against HER, and dendritefree Zn deposition.

In this work, the construction of an anionic MOF ASEI on Zn anodes via a room-temperature self-assembly method has been successfully established. Through coordination interactions, the robust ASEI layer is tightly adhered to the surface of the Zn metal, ensuring good reliability during battery operation. It possesses a high intrinsic Zn2+ conductivity and an increased Zn²⁺ transference number by virtue of the abundant sulfonate groups in the channels. Moreover, under the protection of the ASEI, the ZSB@Zn anode demonstrates enhanced stability against HER and alleviates self-discharge of the full cells. We also find that the Zn²⁺-rich environment with zincophilic sites in the ASEI facilitates high redox kinetics and thus effectively promotes the rate performance of the battery. The consecutive sulfonate groups in the anionic channels of the ASEI also regulate a uniform Zn deposition, which is verified by the combination of experimental characterizations and DFT computations. Consequently, the ZSB@Zn symmetric cell demonstrates an unrivaled plating/stripping cycling lifespan of over 5700 h. The as-developed ZSB@Zn anode further enables NVO full cells with high capacity, excellent rate performance, and longterm cycling stability that is far superior to the counterpart with a bare Zn anode. This simple yet effective strategy for the construction of a MOF ASEI layer on metallic anodes opens up a fresh route toward advanced energy storage systems for practical applications.

ASSOCIATED CONTENT

Solution Supporting Information

The Supporting Information is available free of charge at https://pubs.acs.org/doi/10.1021/acsenergylett.2c01958.

Experimental methods, figures of the illustration for the designing concept and synthesis of the MOF-based ASEI, SEM images of the anodes, XRD patterns, structures, FTIR spectra, contact angles, transference number, and additional electrochemical results for the cells, and tables of data of the microhardness test, transference number, and references in Figure 3e (PDF)

MOF ASEI can remain intact under vigorous bending and scratching (MP4)

Topography change of the bare Zn anode during galvanostatic Zn deposition (MP4)

Topography change of the ZSB@Zn anode during galvanostatic Zn deposition (MP4)

AUTHOR INFORMATION

Corresponding Authors

Ziqi Wang — Department of Materials Science and Engineering, College of Chemistry and Materials Science and Guangdong Provincial Key Laboratory of Functional Supramolecular Coordination Materials and Applications, Jinan University, Guangzhou 510632, P. R. China; Email: wangzq@ jnu.edu.cn

Hongyan Li — Department of Materials Science and Engineering, College of Chemistry and Materials Science, Jinan University, Guangzhou 510632, P. R. China; orcid.org/0000-0002-7073-5198; Email: lihongyan@jnu.edu.cn

Feng Pan — School of Advanced Materials, Peking University Shenzhen Graduate School, Shenzhen 518055, PR China; orcid.org/0000-0002-8216-1339; Email: panfeng@pkusz.edu.cn

Authors

Huige Chen – Department of Materials Science and Engineering, College of Chemistry and Materials Science, Jinan University, Guangzhou 510632, P. R. China

Huashan Wang – Department of Materials Science and Engineering, College of Chemistry and Materials Science, Jinan University, Guangzhou 510632, P. R. China

Weiyuan Huang — School of Advanced Materials, Peking University Shenzhen Graduate School, Shenzhen 518055, PR China

Complete contact information is available at: https://pubs.acs.org/10.1021/acsenergylett.2c01958

Notes

The authors declare no competing financial interest.

ACKNOWLEDGMENTS

This work is supported by the National Natural Science Foundation of China (52102255), the Guangdong Basic and Applied Basic Research Foundation (2022A1515010745, 2020A1515110611, and 2021A1515010362), the Guangzhou Basic and Applied Basic Research Foundation (202201010492), the Fundamental Research Funds for the Central Universities (21621034), and the Open Fund of Guangdong Provincial Key Laboratory of Functional Supramolecular Coordination Materials and Applications (2020B09).

REFERENCES

- (1) Wang, W.; Huang, G.; Wang, Y.; Cao, Z.; Cavallo, L.; Hedhili, M. N.; Alshareef, H. N. Organic Acid Etching Strategy for Dendrite Suppression in Aqueous Zinc-Ion Batteries. *Adv. Energy Mater.* **2022**, 12, 2102797.
- (2) Zhao, Q.; Ding, S.; Song, A.; Qin, R.; Pan, F. Tuning Structure of Manganese Oxides to Achieve High-performance Aqueous Zn Batteries. *Chin. J. Struct. Chem.* **2020**, *39* (3), 388–394.
- (3) Yang, Q.; Li, Q.; Liu, Z.; Wang, D.; Guo, Y.; Li, X.; Tang, Y.; Li, H.; Dong, B.; Zhi, C. Dendrites in Zn-Based Batteries. *Adv. Mater.* **2020**, *32*, 2001854.
- (4) Park, J. H.; Kwak, M. J.; Hwang, C.; Kang, K. N.; Liu, N.; Jang, J. H.; Grzybowski, B. A. Self-Assembling Films of Covalent Organic Frameworks Enable Long-Term, Efficient Cycling of Zinc-Ion Batteries. *Adv. Mater.* **2021**, *33*, 2101726.
- (5) Zhang, Y.; Howe, J. D.; Ben Yoseph, S.; Wu, Y.; Liu, N. Unveiling the Origin of Alloy-Seeded and Nondendritic Growth of Zn for Rechargeable Aqueous Zn Batteries. *ACS Energy Lett.* **2021**, *6*, 404–412.
- (6) Jia, H.; Wang, Z.; Tawiah, B.; Wang, Y.; Chan, C. Y.; Fei, B.; Pan, F. Recent Advances in Zinc Anodes for High-Performance Aqueous Zn-Ion Batteries. *Nano Energy* **2020**, *70*, 104523.
- (7) Verma, V.; Kumar, S.; Manalastas, W.; Srinivasan, M. Undesired Reactions in Aqueous Rechargeable Zinc Ion Batteries. *ACS Energy Lett.* **2021**, *6*, 1773–1785.
- (8) Xu, K. Electrolytes and Interphases in Li-Ion Batteries and Beyond. Chem. Rev. 2014, 114, 11503-11618.
- (9) Quartarone, E.; Mustarelli, P. Electrolytes for Solid-State Lithium Rechargeable Batteries: Recent Advances and Perspectives. *Chem. Soc. Rev.* **2011**, *40*, 2525–2540.
- (10) Wu, H.; Jia, H.; Wang, C.; Zhang, J.; Xu, W. Recent Progress in Understanding Solid Electrolyte Interphase on Lithium Metal Anodes. *Adv. Energy Mater.* **2021**, *11*, 2003092.
- (11) Li, N.; Yin, Y.; Yang, C.; Guo, Y. An Artificial Solid Electrolyte Interphase Layer for Stable Lithium Metal Anodes. *Adv. Mater.* **2016**, 28, 1853–1858.
- (12) Du, W.; Ang, E. H.; Yang, Y.; Zhang, Y.; Ye, M.; Li, C. C. Challenges in the material and structural design of zinc anode towards high-performance aqueous zinc-ion batteries. *Energy Environ. Sci.* **2020**, 13, 3330–3360.
- (13) Park, S. H.; Byeon, S. Y.; Park, J. H.; Kim, C. Insight into the Critical Role of Surface Hydrophilicity for Dendrite-Free Zinc Metal Anodes. *ACS Energy Lett.* **2021**, *6*, 3078–3085.
- (14) Liu, M.; Cai, J.; Xu, J.; Qi, K.; Wu, Q.; Ao, H.; Zou, T.; Fu, S.; Wang, S.; Zhu, Y. Crystal Plane Reconstruction and Thin Protective Coatings Formation for Superior Stable Zn Anodes Cycling 1300 h. *Small* 2022, *18*, 2201443.
- (15) Zeng, X.; Xie, K.; Liu, S.; Zhang, S.; Hao, J.; Liu, J.; Pang, W. K.; Liu, J.; Rao, P.; Wang, Q.; Mao, J.; Guo, Z. Bio-inspired design of an insitu multifunctional polymeric solid-electrolyte interphase for Zn metal anode cycling at 30 mA cm⁻² and 30 mA h cm⁻². *Energy Environ. Sci.* **2021**, *14*, 5947–5957.
- (16) Kang, L.; Cui, M.; Jiang, F.; Gao, Y.; Luo, H.; Liu, J.; Liang, W.; Zhi, C. Nanoporous CaCO₃ coatings enabled uniform Zn stripping/plating for long-life zinc rechargeable aqueous batteries. *Adv. Energy Mater.* **2018**, *8*, 1801090.
- (17) Liang, P.; Yi, J.; Liu, X.; Wu, K.; Wang, Z.; Cui, J.; Liu, Y.; Wang, Y.; Xia, Y.; Zhang, J. Highly reversible Zn anode enabled by controllable formation of nucleation sites for Zn-based batteries. *Adv. Funct. Mater.* **2020**, *30*, 1908528.
- (18) Zou, P.; Zhang, R.; Yao, L.; Qin, J.; Kisslinger, K.; Zhuang, H.; Xin, H. L. Ultrahigh-Rate and Long-Life Zinc—Metal Anodes Enabled by Self-Accelerated Cation Migration. *Adv. Energy Mater.* **2021**, *11*, 2100982.
- (19) Zheng, J.; Cao, Z.; Ming, F.; Liang, H.; Qi, Z.; Liu, W.; Xia, C.; Chen, C.; Cavallo, L.; Wang, Z.; Alshareef, H. N. Preferred Orientation of TiN Coatings Enables Stable Zinc Anodes. *ACS Energy Lett.* **2022**, *7*, 197–203.

- (20) Zhao, Z.; Zhao, J.; Hu, Z.; Li, J.; Zhang, Y.; Wang, C.; Cui, G. Long-Life and Deeply Rechargeable Aqueous Zn Anodes Enabled by a Multifunctional Brightener-Inspired Interphase. *Energy Environ. Sci.* **2019**, *12*, 1938–1949.
- (21) Shin, J.; Lee, J.; Kim, Y.; Park, Y.; Kim, M.; Choi, J. W. Highly Reversible, Grain-Directed Zinc Deposition in Aqueous Zinc Ion Batteries. *Adv. Energy Mater.* **2021**, *11*, 2100676.
- (22) Yan, M.; Dong, N.; Zhao, X.; Sun, Y.; Pan, H. Tailoring the Stability and Kinetics of Zn Anodes through Trace Organic Polymer Additives in Dilute Aqueous Electrolyte. *ACS Energy Lett.* **2021**, *6*, 3236–3243.
- (23) Guo, X.; Zhang, Z.; Li, J.; Luo, N.; Chai, G.-L.; Miller, T. S.; Lai, F.; Shearing, P.; Brett, D. J. L.; Han, D.; Weng, Z.; He, G.; Parkin, I. P. Alleviation of Dendrite Formation on Zinc Anodes via Electrolyte Additives. *ACS Energy Lett.* **2021**, *6*, 395–403.
- (24) Horike, S.; Bureekaew, S.; Kitagawa, S. Coordination pillared-layer type compounds having pore surface functionalization by anionic sulfonate groups. *Chem. Commun.* **2008**, 471–473.
- (25) Yuksel, R.; Buyukcakir, O.; Seong, W. K.; Ruoff, R. S. Metal-Organic Framework Integrated Anodes for Aqueous Zinc-Ion Batteries. *Adv. Energy Mater.* **2020**, *10*, 1904215.
- (26) Zhao, K.; Xiang, Y.; Sun, X.; Chen, L.; Xiao, J.; Liu, X. Highly Efficient One-Step Conversion of Fructose to Biofuel 5-Ethoxymethylfurfural Using a UIO-66-SO3H Catalyst. *Front. Chem.* **2022**, DOI: 10.3389/fchem.2022.900482.
- (27) Naseri, A. M.; Zarei, M.; Alizadeh, S.; Babaee, S.; Zolfigol, M. A.; Nematollahi, D.; Arjomandi, J.; Shi, H. Synthesis and application of [Zr-UiO-66-PDC-SO3H]Cl MOFs to the preparation of dicyanomethylene pyridines via chemical and electrochemical methods. *Sci. Rep.* **2021**, *11*, 16817.
- (28) Bae, D.; Zhen, S.; Seff, K. Structure of Dehydrated Zn²⁺-Exchanged Zeolite X. Overexchange, Framework Dealumination and Reorganization, Stoichiometric Retention of Monomeric Tetrahedral Aluminate. *J. Phys. Chem. B* **1999**, *103*, 5631–5636.
- (29) Moon, D. J.; Choi, S. J.; Lim, W. T. Crystallographic studies of fully dehydrated partially $\mathrm{Zn^{2+}}$ -exchanged zeolite Y (FAU, Si/Al = 1.56) depending on $\mathrm{Zn^{2+}}$ concentration of aqueous solution during exchange. *J. Porous Mater.* **2018**, 25, 1427–1437.
- (30) Wang, Z.; Tan, R.; Wang, H.; Yang, L.; Hu, J.; Chen, H.; Pan, F. A metal—organic-framework-based electrolyte with nanowetted interfaces for high-energy-density solid-state lithium battery. *Adv. Mater.* **2018**, 30, 1704436.
- (31) Liu, H.; Wang, J.; Hua, W.; Sun, H.; Huyan, Y.; Tian, S.; Hou, Z.; Yang, J.; Wei, C.; Kang, F. Building Ohmic Contact Interfaces toward Ultrastable Zn Metal Anodes. *Adv. Sci.* **2021**, *8*, 2102612.
- (32) Evans, J.; Vincent, C. A.; Bruce, P. G. Electrochemical measurement of transference numbers in polymer electrolytes. *Polymer* 1987, 28, 2324–2328.
- (33) Yan, H.; Li, S.; Nan, Y.; Yang, S.; Li, B. Ultrafast Zinc—Ion—Conductor Interface toward High-Rate and Stable Zinc Metal Batteries. *Adv. Energy Mater.* **2021**, *11*, 2100186.
- (34) Wang, Z.; Huang, W.; Hua, J.; Wang, Y.; Yi, H.; Zhao, W.; Zhao, Q.; Jia, H.; Fei, B.; Pan, F. An anionic-MOF-based bifunctional separator for regulating lithium deposition and suppressing polysulfides shuttle in Li—S batteries. *Small Methods* **2020**, *4*, 2000082.
- (35) Ma, L.; Schroeder, M. A.; Pollard, T. P.; Borodin, O.; Ding, M. S.; Sun, R.; Cao, L.; Ho, J.; Baker, D. R.; Wang, C.; Xu, K. Critical Factors Dictating Reversibility of the Zinc Metal Anode. *Energy Environ. Mater.* **2020**, *3*, 516–521.
- (36) Lee, D.; Kim, H.-I.; Kim, W.-Y.; Cho, S.-K.; Baek, K.; Jeong, K.; Ahn, D. B.; Park, S.; Kang, S. J.; Lee, S.-Y. Water-Repellent Ionic Liquid Skinny Gels Customized for Aqueous Zn-Ion Battery Anodes. *Adv. Funct. Mater.* **2021**, *31*, 2103850.
- (37) He, H.; Tong, H.; Song, X.; Song, X.; Liu, J. Highly stable Zn metal anodes enabled by atomic layer deposited Al2O3 coating for aqueous zinc-ion batteries. *J. Mater. Chem. A* **2020**, *8*, 7836–7846.
- (38) Moura, C. A. d. S.; Belmonte, G. K.; Reddy, P. G.; Gonslaves, K. E.; Weibel, D. E. EUV photofragmentation study of hybrid nonchemi-

cally amplified resists containing antimony as an absorption enhancer. *RSC Adv.* **2018**, *8*, 10930–10938.

- (39) Du, M.; Liu, C.; Zhang, F.; Dong, W.; Zhang, X.; Sang, Y.; Wang, J.; Guo, Y.; Liu, H.; Wang, S. Tunable Layered (Na,Mn)V $_8$ O $_{20}$ ·nH $_2$ O Cathode Material for High-Performance Aqueous Zinc Ion Batteries. *Adv. Sci.* **2020**, *7*, 2000083.
- (40) Wang, L.; Huang, K.; Chen, J.; Zheng, J. Ultralong cycle stability of aqueous zinc-ion batteries with zinc vanadium oxide cathodes. *Sci. Adv.* **2019**, *5*, eaax4279.
- (41) Cao, J.; Zhang, D.; Zhang, X.; Zeng, Z.; Qin, J.; Huang, Y. Strategies on regulating Zn²⁺ solvation structure for dendrites-free and side reactions-suppressed zinc-ion batteries. *Energy Environ. Sci.* **2022**, 15, 499–528.
- (42) Hao, J.; Li, B.; Li, X.; Zeng, X.; Zhang, S.; Yang, F.; Liu, S.; Li, D.; Wu, C.; Guo, Z. An In-Depth Study of Zn Metal Surface Chemistry for Advanced Aqueous Zn-Ion Batteries. *Adv. Mater.* **2020**, *32*, 2003021.
- (43) Liu, X.; Yang, F.; Xu, W.; Zeng, Y.; He, J.; Lu, X. Zeolitic Imidazolate Frameworks as Zn²⁺ Modulation Layers to Enable Dendrite-Free Zn Anodes. *Adv. Sci.* **2020**, *7*, 2002173.
- (44) Yu, J.; Lyu, Y.; Liu, J.; Effat, M. B.; Kwok, S. C. T.; Wu, J.; Ciucci, F. Enabling nonflammable Li-metal batteries via electrolyte functionalization and interface engineering. *J. Mater. Chem. A* **2019**, *7*, 17995—18002.
- (45) Luo, S.; Xie, L.; Han, F.; Wei, W.; Huang, Y.; Zhang, H.; Zhu, M.; Schmidt, O. G.; Wang, L. Nanoscale parallel circuitry based on interpenetrating conductive assembly for flexible and high-power zinc ion battery. *Adv. Funct. Mater.* **2019**, *29*, 1901336.
- (46) Li, W.; Han, C.; Wang, Y.; Liu, H. Structural modulation of manganese oxides for zinc-ion batteries. *Chin. J. Struct. Chem.* **2020**, 39 (1), 31–35.

☐ Recommended by ACS

Water Confinement by a Zn²⁺-Conductive Aqueous/Inorganic Hybrid Electrolyte for High-Voltage Zinc-Ion Batteries

Di Luo, Yu Liu, et al.

MARCH 28, 2023

ACS APPLIED ENERGY MATERIALS

READ 🗹

Surface Engineering for Ultrathin Metal Anodes Enabling High-Performance Zn-Ion Batteries

Ziyi Hu, Zijian Hong, et al.

JANUARY 17, 2023

ACS APPLIED MATERIALS & INTERFACES

READ 🗹

A Facile Candle-Soot Nanoparticle Decoration Enables Dendrite-Free Zn Anodes for Long-Cycling Aqueous Batteries

Chenbo Yuan, Shan Gao, et al.

JANUARY 17, 2023

ACS APPLIED ENERGY MATERIALS

READ 🗹

Highly Stable Zn Anodes Modulated by Selenizing In Situ Grown Metal-Organic Frameworks

Yuhan Zou, Jingyu Sun, et al.

DECEMBER 14, 2022

THE JOURNAL OF PHYSICAL CHEMISTRY C

READ 🗹

Get More Suggestions >